

Forced Commutated Controlled Series Capacitor Rectifier for More Electric Aircraft

Tahani Al-Mhana , *Member, IEEE*, Volker Pickert , *Member, IEEE*, David J. Atkinson, and Bashar Zahawi , *Senior Member, IEEE*

Abstract—Rising power demands in more electrical aircraft (MEA) put power converters for commercial airplanes under increasing pressure to fulfill current harmonic distortion regulations as specified, for example, in DO-160G. Today, the implementation of filters is seen as an effective tool for dealing with harmonics; however, their increased weight and volume are not welcomed in the aerospace industry. This paper proposes a circuit, named forced commutation controlled series capacitor (FCSC-rectifier), which is able to maintain low individual harmonic current levels without the need for filter components. The FCSC-rectifier includes a variable capacitive line reactance that interacts in a controlled manner with the inductive line impedance. The result is that the converter input current is nearly purely sinusoidal with a power factor of almost unity. The FCSC-rectifier is to be used for stand-alone variable-voltage, variable-frequency generation systems and can, therefore, power the full authority digital electronic control system (FADEC) in an MEA. This paper shows that the FCSC-rectifier can maintain a high power factor and acceptable current harmonic levels without the use of filters, despite large voltage and frequency variations. A full description of the circuit modes of operation is presented in this paper together with simulation results showing circuit performance characteristics over a range of voltages and frequencies. Results are experimentally verified using a 1-kW test circuit.

Index Terms—Current harmonics, forced commutation controlled series capacitor (FCSC), full authority digital electronic control system (FADEC), more electric aircraft (MEA), power factor.

I. INTRODUCTION

THE complexity of aircraft electrical loads has substantially increased in recent years with the advent of the more electric aircraft (MEA) [1]–[3]. The most safety critical system in any MEA is the full authority digital electronic control (FADEC) system that continuously monitors and controls the ignition timing and fuel injection to the aircraft engine. FADEC control and designs have been reported in [4]–[6] with the focus

Manuscript received June 14, 2017; revised November 24, 2018 and January 11, 2018; accepted March 1, 2018. Date of publication March 14, 2018; date of current version November 19, 2018. Recommended for publication by Associate Editor A. K. Gupta. (*Corresponding author: Volker Pickert.*)

T. Al-Mhana is with the Department of Electrical Engineering, University of Babylon, Hilla 51002, Iraq (e-mail: eng.tahany.hamodi@uobabylon.edu.iq).

V. Pickert and D. J. Atkinson are with the School of Engineering, Newcastle University, Newcastle upon Tyne NE1 7RU, U.K. (e-mail: volker.pickert@ncl.ac.uk; dave.atkinson@ncl.ac.uk).

B. Zahawi is with the Department of Electrical and Computer Engineering, Khalifa University of Science and Technology, Abu Dhabi 127788, United Arab Emirates (e-mail: bashar.zahawi@ku.ac.ae).

Color versions of one or more of the figures in this paper are available online at <http://ieeexplore.ieee.org>.

Digital Object Identifier 10.1109/TPEL.2018.2816305

being mainly on safety. Any failure within the FADEC leads to misfiring and loss of fuel injection [7]–[10], which would result in a catastrophic event, such as the Airbus A 400 M crash in 2015 caused by FADEC failure [11]. One major area of concern is radiated and conducted electromagnetic interference (EMI) which could interact with the engine control hardware. Radiated EMI is minimized by enclosing the FADEC in a metal cage. Conducted EMI is minimized by powering the FADEC from its own variable frequency generator (VFG), minimizing the risk of harmonic contamination from the supply currents when connected to the MEA distribution network. The FADEC is the only stand-alone powered electronic system that has its own VFG in the MEA (there is, however, a dc link connection to a backup system, which is activated in case of the loss of the VFG [12]). As well as producing low harmonics, the VFG must also be reliable, low-cost, power-dense, light in weight, and environmental friendly [13]–[15], as is necessary for all MEA electronic systems.

Today's standard VFG design for FADEC supplies is the series connection of a permanent magnet (PM) generator with a diode bridge rectifier and a dc/dc converter stepping down the voltage to 28 V. The dc/dc converter is designed to cope with load variations caused by the FADEC although variations are small as digital controller boards do not experience large load swings. This principal was proposed in 2009 [12] and is still implemented in today's most advanced MEAs such as the Airbus A 380 and Boeing 787. The combination of a PM generator and a diode bridge rectifier fulfills aerospace requirements in that it is efficient, power-dense, and reliable [16]–[18]. However, the PM generator/diode bridge rectifier combination is known for its current harmonic generation and poor power factor [19].

So far this has not been an issue, as the power requirement of the FADEC hardware is relatively low. Future aircraft, however, will have more complex engines with more electronic hardware and processing needs, requiring higher levels of input power. This, in addition to further increases in the electrification regulatory requirements for commercial aircrafts, such as those specified in DO-160G "Environmental Conditions and Test Procedures for Airborne Equipment," imposed by the Radio Technical Commission for Aeronautics [20], will push the limits of acceptable current harmonic levels.

The DO-160G is a guideline for the standard procedures and criteria of environmental tests for airborne hardware, including electrical and electronic avionics and mechanical systems. It also defines the input harmonics distortion limits caused by

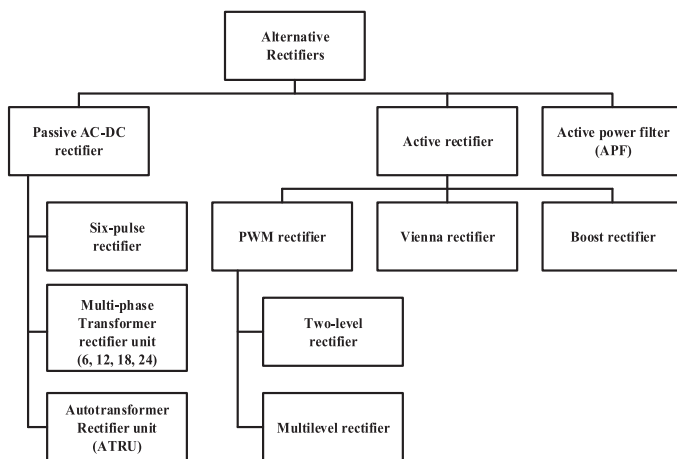


Fig. 1. Overview of rectifiers presented in the literature as an alternative to the diode bridge rectifier.

various loads, due to the recognition of the negative impact of harmonics on aircraft power systems caused mainly by the intensive use of uncontrolled rectifiers in airborne systems. Historically, DO-160G has been updated regularly in line with developments in the MEA industry and PM generators with diode bridge rectifiers are likely to be prohibited in the future due to the ever-tighter limitations on power converter current harmonic distortion.

Consequently, alternative solutions are required for powering stand-alone electrical systems in MEA such as the FADEC. The most obvious approach is the implementation of filters between the PM generator and the diode bridge rectifier. However, this will increase the volume and weight of such a system by about 50% [21] which is not desirable. Other work has focused on the employment of passive and active three-phase high power factor converter topologies [22]–[25]. The use of a transformer rectifier unit [26] or an autotransformer rectifier unit [27] has been investigated to supply a multipulse (12- or 18-pulse) rectified dc voltage. These rectifier units are adapted for current harmonic cancellation to meet DO-160G requirements but at the expense of increased weight and volume [28]. The use of well-established active rectifiers such as the two- and multi-level pulsewidth modulation (PWM) rectifier, and Vienna rectifier have also been investigated [29]–[31]. Although these are able to enhance the power factor without the use of transformers, the control circuit complexity raises safety concerns and the high-power, fast switching requirements result in current harmonics that still require filtering [19], [28], [30]. Current harmonics produced by active front-end converters are determined by many factors such as load, switching frequency, filter design, type of filter, and PWM control strategy [32], [33]. A summary of all rectifiers proposed in the literature as an alternative to the diode bridge rectifier is presented in Fig. 1.

To date, all proposed systems for current harmonic reduction require filtering or additional magnetic components. This paper proposes a power electronic rectifier circuit that produces low current harmonics, fulfilling DO-160G requirements without the need for filters. The new rectifier circuit is referred to in this paper as the forced commutation controlled series capacitor rectifier (FCSC-rectifier). It has a simple control structure and

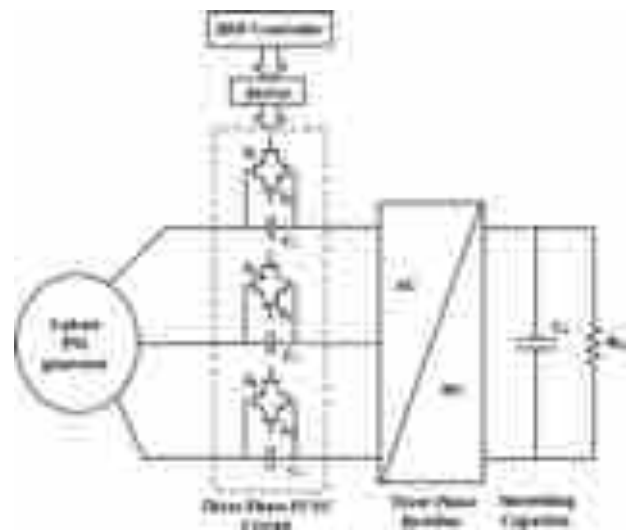


Fig. 2. Three-phase FCSC-rectifier in a stand-alone three-phase generation system.

it operates at a low switching frequency to produce a nearly sinusoidal supply current waveform at a power factor of almost unity. The operation of the proposed FCSC-rectifier is described, simulated and experimentally verified using a 1-kW test circuit.

The remainder of this paper is structured as follows. Section II describes the fundamental principal of the FCSC-rectifier topology. In Section III, the modes of operation of the FCSC-rectifier are presented, including a description of the control method that has been applied. Simulations using Saber/Synopsys are presented in Section IV. The FCSC-rectifier behavior is verified experimentally using a 1-kW laboratory test bench and test waveforms and results are shown in Section V. Current harmonic spectrums (experimental and simulated waveforms) are shown in Section VI and a conclusion is presented in Section VII.

II. FCSC-RECTIFIER CIRCUIT TOPOLOGY

The FCSC-rectifier is shown in Fig. 2, situated between the aircraft three-phase PM generator and the on-board dc load (shown in the figure as an equivalent resistor). The three-phase FCSC-rectifier is comprised of a three-phase, forced commutation controlled capacitor circuit in series with a three-phase diode bridge rectifier. In each phase, a series compensation capacitor C_c is connected in parallel to two antiparallel insulated gate bipolar transistor (IGBT) switches used to control the injected series capacitive reactance. The aim is to match the effective capacitive reactance with the generator inductive reactance to achieve high power factor and minimum current distortion for a wide range of operating frequencies, thus avoiding the need for additional filtering.

The FCSC-rectifier is based on the topology used in flexible ac transmission system (FACTS) controllers in power system applications, where ac voltages and frequencies are generally stable [34]–[36]. The purpose of the FCSC circuit in FACTS applications is to inject a small capacitive reactance into the transmission lines for grid quality purposes [37], [38]. The IGBTs are switched-on at the zero-crossing point of the supply voltage and the turn-off time is calculated based on the required amount of injected capacitive reactance.

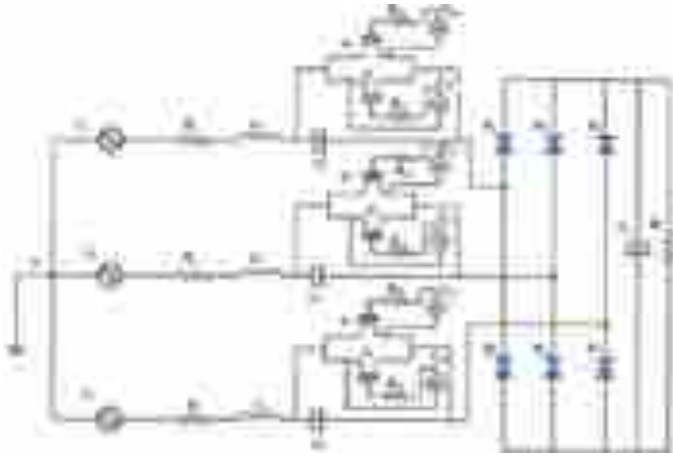


Fig. 3. Schematic diagram of the three-phase FCSC-rectifier.

The proposed FCSC-rectifier is different from the FACTS conventional circuit in several ways. First, it is designed for stand-alone applications, embedded between an ac generator and a dc output stage. Second, an ac current is injected into the rectifier as the effective capacitive reactance and can be controlled by varying the on-state time of the IGBT switches and resonance is achieved by tuning the phase capacitive reactance to the same value of the inductive reactance of the PM generator. This operational point has two advantages: a near sinusoidal ac current waveform with low current harmonics and a high input power factor, as the current is in phase with the generator phase-voltage. It is perhaps worth noting that the operation of the input stage of the FCSC-rectifier cannot be compared directly with a classical RLC resonant circuit. This is because the series capacitor C_c is switched via the action of the IGBTs and the voltage across the capacitor is not always part of the series resonant circuit formed by the generator inductance, generator resistance, and C_c . Finally, FCSCs in FACTS applications operate with small ac input variations (typically $\pm 1\%$ variation of nominal frequency and $\pm 10\%$ of nominal voltage) [39] whereas the FCSC-rectifier has to deal with the full range of output voltage fluctuation and frequency variation produced from the VFG. As the operation of the FCSC-rectifier is fundamentally different to that of the FCSC, the control strategy must also be different. This is discussed in the following section.

III. MODES OF OPERATION AND CONTROL METHOD

Fig. 3 shows a three-phase FCSC-rectifier with its input connected to the three-phase generator and its output connected to a load capacitor C_L in parallel with a load resistor R_L . In this figure, the three-phase PM generator is represented by a set of balanced three-phase voltage sources (v_a, v_b, v_c), in series with three identical impedances (internal resistance R_s and inductance L_s) in each phase. The phase voltages in this balanced three-phase system are given by

$$\begin{aligned} v_a &= V_{\max} \sin(\omega t) \\ v_b &= V_{\max} \sin(\omega t - 2\pi/3) \\ v_c &= V_{\max} \sin(\omega t - 4\pi/3) \end{aligned} \quad (1)$$

where V_{\max} is the amplitude of the sinusoidal generator induced voltage.

Each phase includes a series connected compensation capacitor C_C whose value is chosen in accordance with the generator inductance to insure resonance at the maximum operating supply frequency (f_{\max}) [40]

$$f_{\max} = f_r = \frac{1}{2\pi\sqrt{L_s C_C}} \quad (2)$$

where f_r is the resonance frequency. The value of C_c can then be determined from the following formula:

$$X_{CC}|_{f_s=f_{\max}} = X_{c\max} = \frac{1}{2\pi \times f_{\max} \times C_c}. \quad (3)$$

Resonance can be achieved by controlling the duty ratio of the IGBT switches in accordance with the supply frequency value. When the operating frequency is reduced, the controller increases the duty ratio of the switches (the capacitor is bypassed by the IGBTs for a longer period) and the effective capacitive reactance $X_{cc,\text{eff}}$ is reduced [41] in line with the reduction in X_{LS} maintaining the condition

$$X_{CC,\text{eff}} = X_{LS} = \omega L_s \quad (4)$$

where ω is the electric angular frequency produced by the generator.

$X_{CC,\text{eff}}$ is determined by the capacitor C_C and the conduction period δ of the associated IGBTs. The duty ratio (D) for each active switch can be calculated as

$$D = \frac{\delta}{2\pi}. \quad (5)$$

In one full cycle, the capacitor will be short circuited twice by the corresponding pair of IGBT switches. The effective capacitive reactance is then given by

$$X_{cc,\text{eff}} = (1 - 2D) \times X_{c\max} \quad (6)$$

by substituting (4) in (6), we obtain

$$X_{LS} = (1 - 2D) \times X_{c\max}. \quad (7)$$

Equation (7) can be rewritten as

$$D = \frac{1}{2} \left(1 - \frac{X_{LS}}{X_{c\max}} \right). \quad (8)$$

Giving the relationship

$$D = \frac{1}{2} \left(1 - \frac{f_s}{f_{\max}} \right). \quad (9)$$

The duty cycle D for each frequency variation is calculated using (9). In the practical implementation of the circuit, the microcontroller calculates the new duty-cycle based on the frequency f_s of the previous cycle. The frequency f_s is determined using a zero-crossing detection (ZCD) circuit and, therefore, the ZCD triggers the calculation of the conduction period δ , which can be calculated from (5) and (9)

$$\delta = \pi \left(1 - \frac{f_s}{f_{\max}} \right). \quad (10)$$

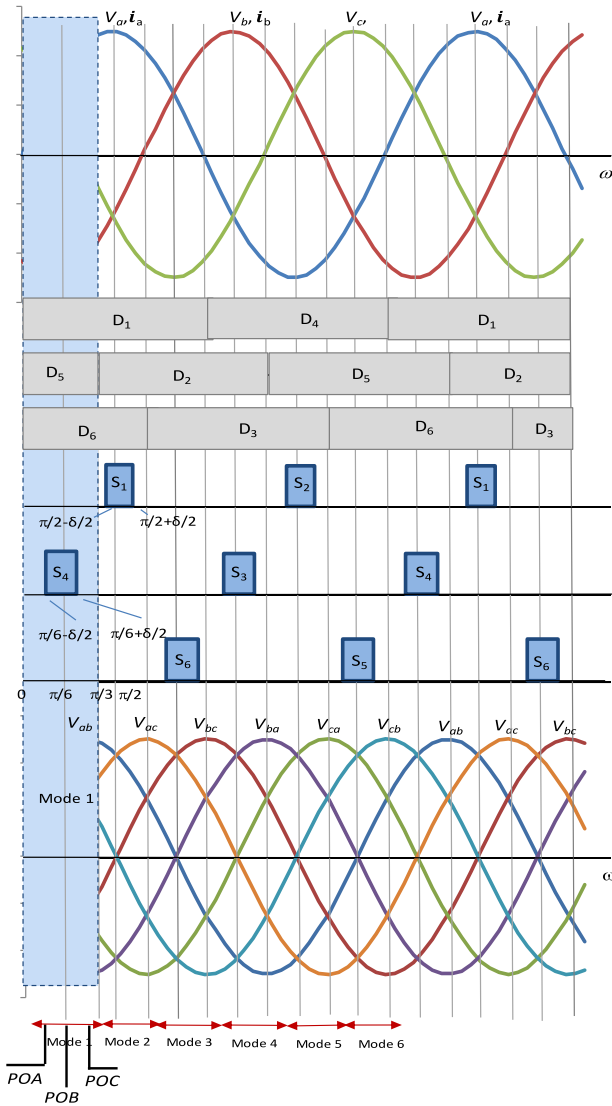


Fig. 4. Operational modes, switching states, and normalized voltage and current waveforms of the three-phase FCSC-rectifier.

Thus, all switches are synchronized to the ZCD trigger event and, therefore, the FCSC-rectifier only requires a low-cost microcontroller to deal with MEA's VFG range. By applying the correct duty cycle, the resonance condition expressed in (4) is achieved and the generator current waveform is maintained in-phase with the generator voltage waveform resulting in almost unity power factor operation.

Fig. 4 displays the timing diagram and the various modes of operation of the circuit, showing the diode conducting periods together with the switching patterns of all IGBT switches. During the positive half-cycles of the three-phase generator voltage, switches S_1 , S_3 , and S_5 are ON (and during the negative half-cycle S_2 , S_4 , and S_6 are ON) for an interval δ that is symmetrically centered around the peak of the generator voltage waveform.

Each IGBT has a conduction period of δ , which can vary from $\delta = 0$ to $\delta = \pi/2$. The IGBT ON time is varied in line with the supply frequency variations. At resonance, each phase produces

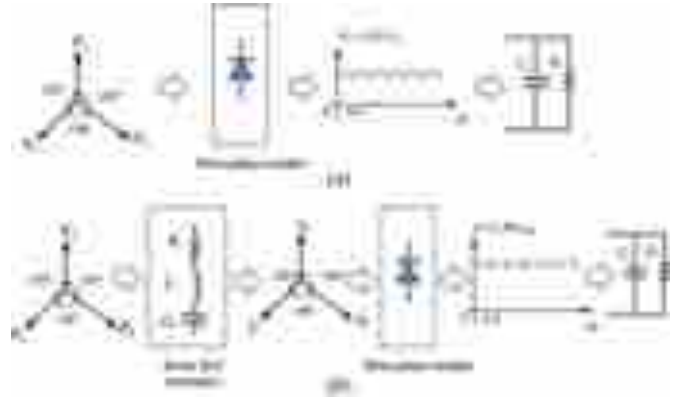


Fig. 5. Comparison of operating characteristics. (a) Classical voltage-fed rectifier. (b) FCSC-rectifier.

a pure sinusoidal ac current waveform

$$\begin{aligned} i_a &= I_{\max} \sin(\omega t) \\ i_b &= I_{\max} \sin(\omega t - 2\pi/3) \\ i_c &= I_{\max} \sin(\omega t - 4\pi/3) \end{aligned} \quad (11)$$

where I_{\max} is the amplitude of the sinusoidal phase current.

Fig. 4 shows the total current is always zero because the system is balanced. The state of conduction of the diodes depends on the direction of the phase currents (the upper diodes D_1 , D_3 , D_5 conduct when the corresponding phase current is positive and the lower diodes D_2 , D_4 , D_6 conduct when the current is negative). As the FCSC-rectifier operates on the basis of phase current injection when running at resonance, the diode commutation process is different from that found in classical voltage-fed rectifiers. In the latter, commutation takes place between neighboring diodes (from one conducting leg to the neighboring leg). In the FCSC-rectifier, however, diode commutation always takes place between the upper and the lower diodes in the same leg, resulting in the six-pulse dc current waveform shown in Fig. 5, in which the operation of the FCSC-rectifier is compared with that of a conventional three-phase diode bridge rectifier.

Each mode shown in Fig. 4 (Modes 1 to 6) lasts for a period of $\pi/3$ and corresponds to a given diode conduction pattern. Due to symmetry, each mode has the same repeating principal operations (referred to here as POA, POB, and POC). These are discussed below for Mode 1.

A. Principle Operation A (POA): $0 < \omega t < \pi/6 - \delta/2$: D_1 , D_5 , and D_6 Conduct

Fig. 6 shows the circuit at the start of Mode 1. In this figure, the R_L - C_L load is represented as a single unit for simplicity. Mode 1 starts at $\omega t = 0$ (using v_a as a reference, as shown in Fig. 4). At the start of this period, no switch has been activated and diodes D_1 , D_5 , and D_6 are conducting. As the effective overall capacitive reactance $X_{cc,eff}$ over the full cycle is equal to X_{LS} , the currents i_a , i_b , and i_c are in phase with the voltages v_a , v_b , and v_c , respectively. In this mode, i_a and i_c are positive flowing into the diode bridge rectifier and i_b is negative (see Fig. 4). The currents i_a , i_b , and i_c are given by (12) and the load

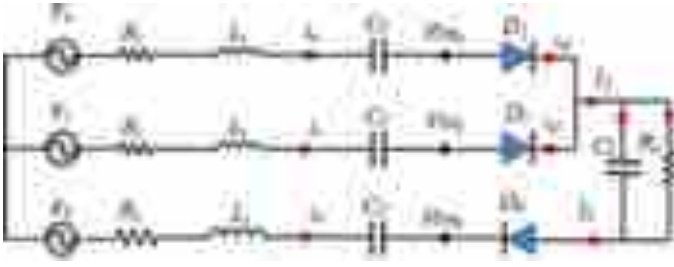


Fig. 6. Effective circuit during POA.

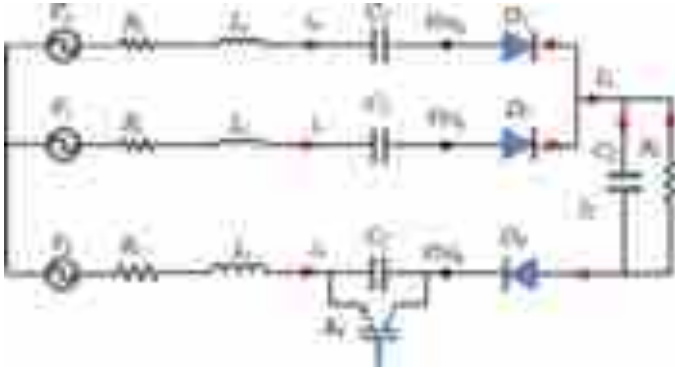


Fig. 7. Effective circuit during POB.

current I_L can be determined from Kirchoff's current law

$$I_L = i_a + i_c = I_{\max} \sin(\omega t - 2\pi/3). \quad (12)$$

B. Principal Operation B (POB):

$\pi/6 - \delta/2 < \omega t < \pi/6 + \delta/2$: S_4 ON, D_1 , D_5 , and D_6 Conduct

At $\omega t = \pi/6 - \delta/2$, S_4 is turned ON and all other IGBTs are OFF (see Fig. 7). S_4 is ON during this period, short circuiting C_C in phase-b. However, since $X_{cc,eff}$ is still adjusted over the full cycle to be equal to X_{LS} , i_a and i_c are still in phase with v_a and v_c , respectively, and phase-b provides the return path for i_a and i_c

$$i_b = -i_a - i_c. \quad (13)$$

Despite the short circuiting of the capacitor C_C in phase-b, a resonant current is injected in phase-b which is in phase with the voltage v_b (see Fig. 4). The load current I_L can still be determined from Kirchoff's current law and (12).

C. Principal Operation C (POC): $\pi/6 + \delta/2 < \omega t < \pi/3$: D_1 , D_2 , and D_6 Conduct

At $\omega t = \pi/6 + \delta/2$, S_4 is turned OFF and all remaining IGBTs are OFF. The circuit is identical to that shown in Fig. 6 and circuit operation is identical to POA.

At $\omega t = \pi/3$ Mode 2 starts as v_c becomes negative and the current in phase-c changes polarity. The current in diode D_5 commutates to D_2 , as shown in Fig. 4.

TABLE I
CIRCUIT PARAMETERS

Circuit parameter	Value
V_S	75–100 V
f_S	240–480 Hz
R_s	2.5 Ω
L_s	13.75 mH
C_C	8 μ F
C_L	500 μ F
R_L	30 Ω

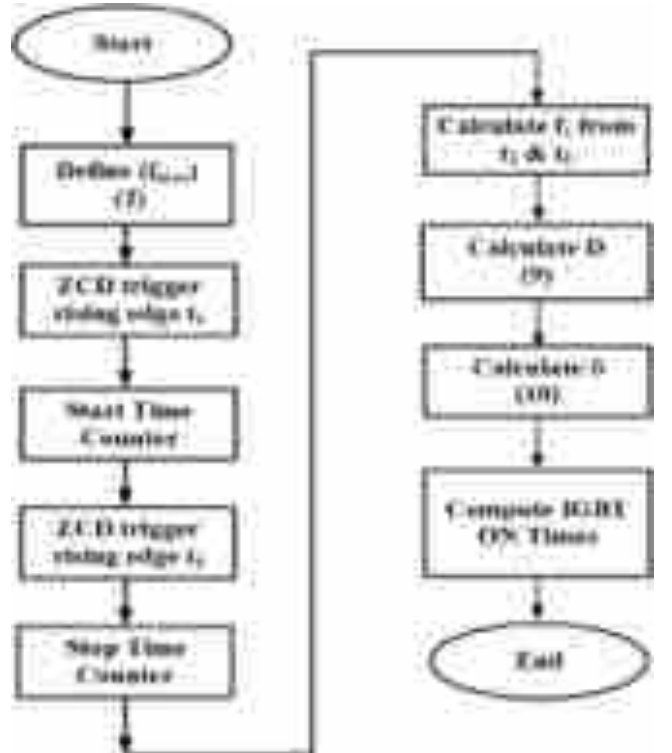


Fig. 8. Flowchart for computing IGBT switching times (t_1 : timing when supply voltage crosses zero, t_2 : timing when supply voltage crosses zero for the second time).

IV. SIMULATION RESULTS

To allow for direct comparisons with experimental tests, the FCSC-rectifier circuit is simulated in Saber using the parameters of the experimental test rig listed in Table I. Generator parameters are based on an aero engine generator described in [42] and [43]. The simulations are carried out for a frequency/voltage range between (240–480 Hz)/(75–100 V) to comply with the minimum/maximum frequency/voltage of the programmable power source used in the practical test. At the maximum frequency of 480 Hz, with a voltage of 100 V, all the IGBT switches are permanently OFF. Below this frequency, the IGBTs are controlled to obtain a conduction period δ based on (10). Fig. 8 shows a summary of steps required to calculate the IGBTs ON and OFF times. Fig. 9 shows the high level block diagram of the circuit simulation model.

Simulation results for the FCSC-rectifier operating at a typical aircraft frequency of 400 Hz (also known as the nominal

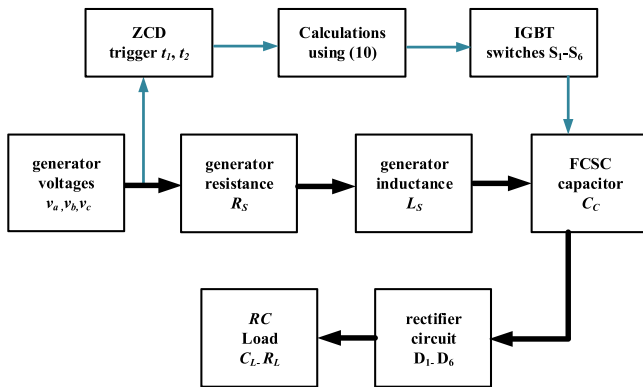


Fig. 9. Block diagram of circuit simulation model (black arrows: power, blue arrows: signal).

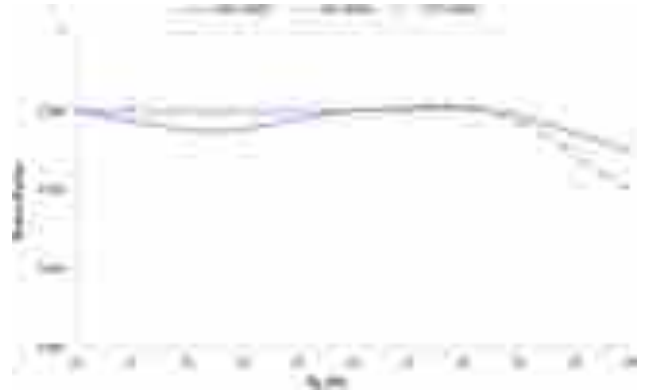


Fig. 11. FCSC-rectifier power factor as a function of PM generator voltage and frequency under various load conditions (simulated results).

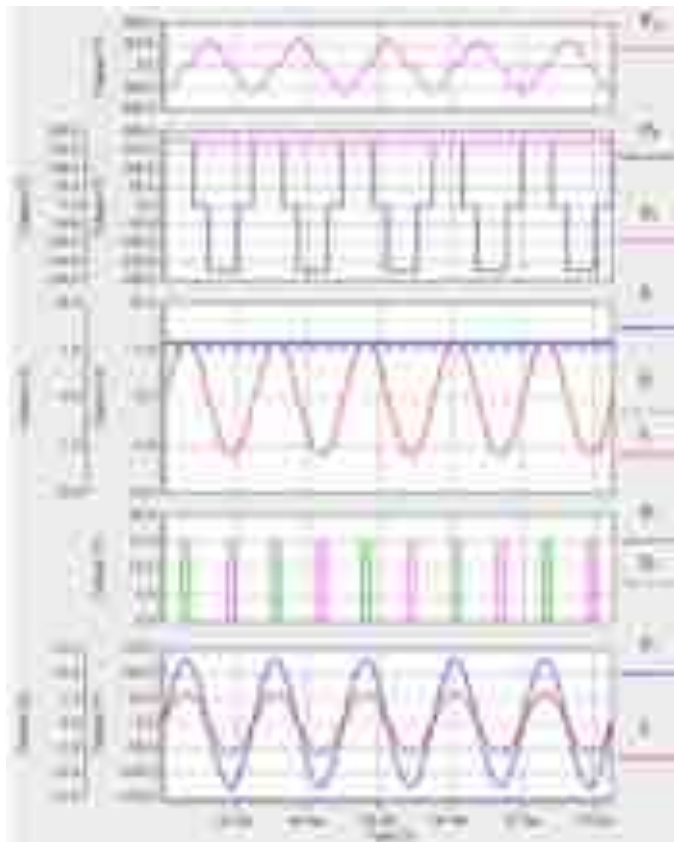


Fig. 10. Three-phase FCSC-rectifier waveforms at 90 V/400 Hz (simulated). V_{cc} : voltage across the capacitor, V_{in} : line-to-line input voltage of the three-phase rectifier (diode bridge), V_L : load voltage, I_L : load current, i_L : output current of the three-phase rectifier, i_s : supply current, V_s : supply voltage.

frequency [13], [30]) are shown in Fig. 10. The figure shows that the series capacitor can maintain the input current in-phase with the voltage waveform, so that the power factor is maintained at a high value. The rectifier input voltage V_{in} is clamped by the load voltage and the rectifier output current (i_L) consists of six pulses of the ac phase currents, as described in Section III. The average dc load current also complies with the relationship $I_L = 1.35 I_{RMS}$. The voltage across the series capacitor is zero as long as the corresponding IGBTs are in the ON state.

Fig. 11 shows the operating power factor of the circuit plotted against variations in load for three different voltage/frequency

TABLE II
SENSITIVITY STUDY

Load	10% error in	PF-10%	PF
$R_L = 10 \Omega$	L_S	0.902	0.997
	C_C	0.916	0.997
$R_L = 20 \Omega$	L_S	0.962	0.998
	C_C	0.968	0.998

TABLE III
UNBALANCED OPERATION

Load	10% imbalance in	PF-10%	PF
$R_L = 10 \Omega$	L_S	0.963	0.997
	C_C	0.961	0.997
$R_L = 20 \Omega$	L_S	0.937	0.998
	C_C	0.918	0.998

conditions. The FCSC-rectifier maintains a high power factor for all voltage/frequency values with a minimum value of 0.99. The highest power factor of 0.998 is achieved at the highest voltage/frequency values (100 V/480 Hz) under heavy load conditions and the lowest power factor occurs at the lowest voltage/frequency values (75 V/240 Hz) under light load conditions. The output capacitor C_L represents the input stage of a dc/dc converter that would normally be connected to the output of the diode bridge rectifier of the FADEC and is, therefore, simulated as a constant value. Unlike in a classical diode bridge rectifier where C_L experiences periodical current charging spikes flowing from the ac supply C_L in the FCSC-rectifier experiences a six-pulse dc current waveform, as shown in Fig. 10. Each pulse lasts for 60° independently of the input frequency and the load. Changes in C_L values have no noticeable impact on the operation of the circuit but will affect the ripple content of load voltage and load current.

A sensitivity study (see Table II) and a study of unbalanced operation (see Table III) was conducted for 100 V/480 Hz operation at two load conditions: full load $R_L = 10 \Omega$ and half load $R_L = 20 \Omega$. In the sensitivity analysis, a 10% error in the values of either L_s or C_C was applied to all three phases. For unbalanced operation, a 10% imbalance in the values of either

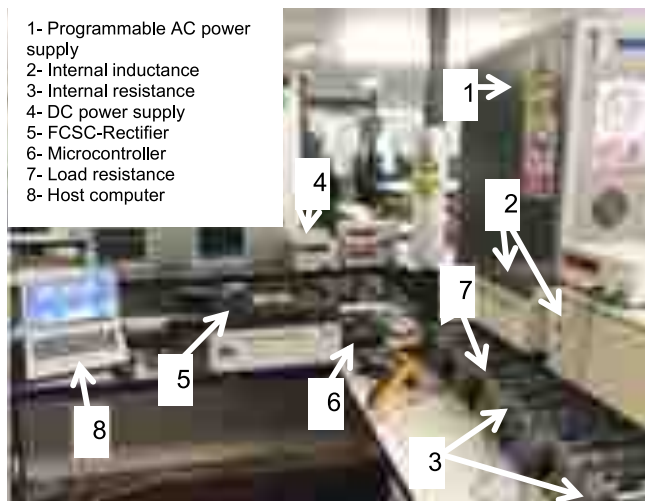


Fig. 12. Photograph of the experimental test rig.



Fig. 13. Photograph of the FCSC-rectifier.

L_s or C_C was considered as well as an imbalance in the supply voltages ($v_a = 100$ V, $v_b = 120$ V, and $v_c = 110$ V).

The third column [power factor (PF)-10%] in both tables shows the resulting PF values, whereas the values in the fourth column are the PFs with no errors or imbalances. Errors and imbalances clearly reduce the PF values that could be achieved, but they do not alter the fundamental operation of the circuit. Table II shows that the highest drop in PF (from 0.997 to 0.902) is at $R_L = 10 \Omega$ and a 10% error in L_s . The highest drop in PF in Table III (from 0.998 to 0.918) is at $R_L = 20 \Omega$ and a 10% imbalance in C_C . Generator voltages imbalance ($v_a = 100$ V, $v_b = 120$ V, and $v_c = 110$ V) produced no measurable change in PF. This is because the displacement factor is independent of the voltage supply amplitude.

In the rare event that any of the phase capacitors C_c become short circuited or open circuited, all switches S_1 to S_6 will be turned ON continuously and the circuit morphs into a diode bridge rectifier connected to a permanent magnet synchronous generator (PMSG). The same applies if any of the switches become short circuited. In the case of an open-circuit fault in any of the switches, all devices will be turned OFF continuously. As with any fault, the operating PF will be affected but the FCSC-rectifier will still be able to deliver power to the FADEC.

V. EXPERIMENTAL VALIDATION

The behavior of the three-phase FCSC-rectifier was experimentally verified under various operating conditions using a 1-kW laboratory test bench. A photograph of the test bed is shown in Fig. 12. All recorded ac measurements were captured for phase-a only. The test hardware consisted of three major parts. The PM generator was emulated using 60 KVA Behlman programmable ac power supply with an internal inductive and resistive impedance to emulate the PM generator. This power supply was used to provide the system with variable-voltage and variable-frequency power over a frequency range between (240–480 Hz). The second part is the conversion stage (inside the enclosure) including the three-phase FCSC-rectifier. Three dual-gate driver circuits were used to provide the pulses required

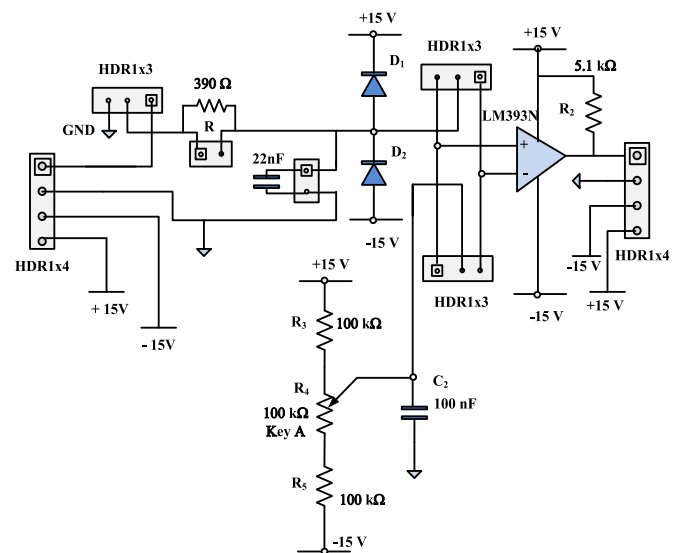


Fig. 14. Zero-crossing detection circuit.

to drive the IGBT switches. The voltage and current sensor cards were also placed inside the enclosure with the ZCD card, as shown in Fig. 13. The ZCD circuit is shown in Fig. 14. It includes an RC low-pass filter to prevent spurious ZCDs caused by the ac source distortion (22 nF and 390 Ω resistor). An LM393N comparator is used to produce the square wave output voltage signal by comparing the filtered voltage signal with a reference voltage. A 100-kΩ potentiometer was provided in order to adjust the pulsewidth as required. The readings of the current sensors and the ZCD card were fed to the microcontroller to be processed. Finally, the controller was based on a TMS320F28335 Texas Instruments DSP mounted on a general interface board. A host computer was required to provide an environment in which to debug the software. A National Instruments LabView package was used for monitoring and control purposes. The resistive load was fed from the output of the three-phase rectifier. Table IV summarizes the specifications of the experimental test rig and the main components of the FCSC-rectifier. The total volume

TABLE IV
EXPERIMENTAL RATING SPECIFICATION AND COMPONENTS
OF THE FCSC-RECTIFIER

Rating specification of the FCSC-rectifier			
Parameters	Specifications		
Input voltage	Variable three-phase RMS (phase-neutral), 75–100 V		
Input frequency	Variable frequency of 240–480 Hz		
Load power	1 kW		
Main components employed in the 1-kW FCSC-rectifier			
Symbol	Manufacturer	Part Number	Typical data
C_C	General electric	97F8248 (Polypropylene film)	8 μ F, 660 V ac
S_1 – S_6	IXYS	IXDR 30N120	1200 V, 50 A
D_1 – D_6	IXYS	VU062-16NO7	1600 V, 63 A
C_L	Panasonic	EETEE2W251LJ (Electrolytic)	2 \times 250 μ F, 450 V

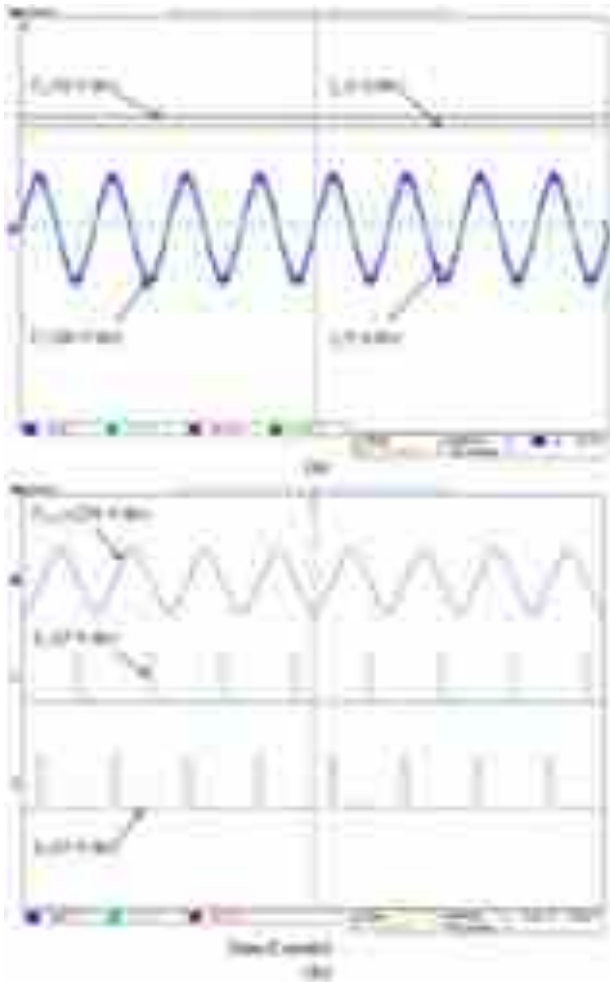


Fig. 15. Experimental FCSC-rectifier waveforms at 90 V/400 Hz.

of the power components used in the test circuit is 1090.85 cm³ and the weight (without heatsink) is 931.3 g.

Fig. 15 shows the recorded experimental results for operation at typical aircraft frequency of 400 Hz and a voltage of 90 V. Waveforms for line-to-neutral supply voltage V_s , the input current i_s , dc load voltage V_L , and dc load current I_L are shown, as well as the voltage across the series capacitor V_{CC} and the

pulses supplied to the switches S_1 and S_2 through one dual driving circuit board. The supply current is almost sinusoidal with an RMS value of about 3.5 A, and is practically in-phase with the supply voltage v_s confirming the effectiveness of the control strategy in matching the effective capacitive reactance to the generator inductive reactance. The dc load voltage is constant at 160 V because of the presence of the load capacitor C_L . The figure also shows the switch timing pulses and the resulting series capacitor voltage, which is zero when S_1 or S_2 are closed in each half-cycle of the supply voltage waveform.

The same system behavior is observed when comparing simulation and experimental results; however, the experimental results show differences in the magnitudes of voltage and current compared with simulations. For example, the load voltage in Fig. 15 is 130 V (experimental) whereas the load voltage in Fig. 10 is 170 V (simulation). The highest errors between simulation and experimental values occur at the highest voltage and frequency of 100 V/480 Hz with a 22.9% difference in the values of average load voltage V_L . This error decreases at lower frequencies. The differences can be explained by the extra losses in the experimental test circuit due to the use of passive components (inductors L_S and series capacitors C_C) designed to be employed at 50 Hz. To support this statement, the FCSC-rectifier was operated at 50 V/50 Hz. The error between measurement and simulation at 50 Hz was reduced in this case to below 5%. This confirms that inductor core loss and capacitor losses in the test rig are responsible for the discrepancy between experimental and simulated results when operated at frequencies above 50 Hz. This observation has been previously reported [44] in power factor correction applications with switching converters. An accurate calculation of inductor loss is highly challenging in applications where the frequency or the duty cycle are variable since conventional methods for core loss estimation based on manufacturer's data sheets cannot be used in such cases. In an aircraft installation, the PM generator will be specifically designed to operate over the required range of frequencies and care will be taken to reduce machine losses to a minimum. For example, in [42] and [45], core losses are reduced by using a segmented stator PM alternator to reduce the magnetic wedges, which affect the eddy current loss.

Fig. 16 shows the measured relationship among power factor, load, and voltage/frequency. This figure clearly shows that the input power factor is high at all values of supply voltage and frequency. The highest power factor (0.99) was achieved at the higher voltage/frequency of 100 V/480 Hz. The minimum value of power factor (0.95) occurred at minimum load, recorded at 75 V/240 Hz. The figure also shows that the variation in load resistance has a small impact on the power factor.

VI. HARMONIC AND EFFICIENCY ANALYSIS

Since the three-phase FCSC-rectifier is being proposed for aircraft applications, it is imperative to examine the ac current harmonic spectrum as a function of load variations. This is important due to the strict limits placed on individual harmonics in such applications. In this section, the harmonic components of the simulated and experimental ac current waveforms are calculated using fast Fourier transform analysis, up to the 40th har-

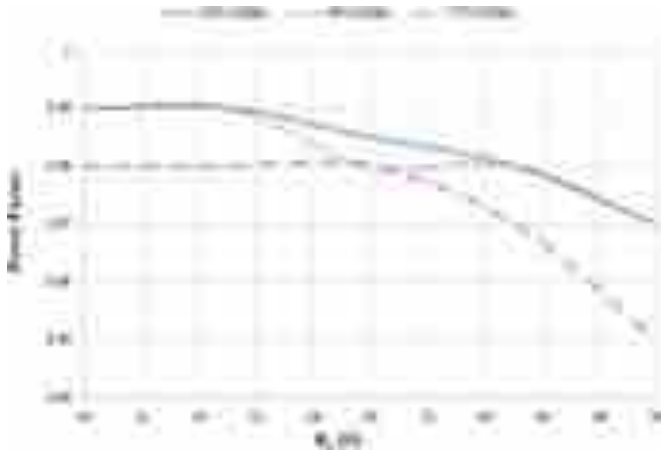


Fig. 16. FCSC-rectifier power factor as a function of PM generator voltage and frequency under various load conditions (experimental results).

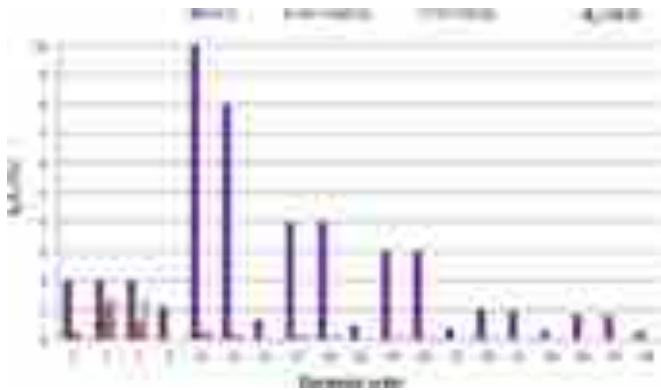


Fig. 17. Input current harmonic spectrum as a function of V_S/f_S ; simulated waveforms, $R_L = 20 \Omega$.

monic as required in MEA standards. Results are compared with the demands imposed by DO-160G, as listed in [26], to examine the suitability of the FCSC-rectifier in an aircraft application. Harmonic spectra are presented at minimum voltage/frequency and at maximum voltage/frequency. In addition, operation at two load conditions $R_L = 20 \Omega$ and $R_L = 10 \Omega$ (emulates a load change of 50%).

A. Harmonic Spectrum (Simulation Results)

Fig. 17 compares simulation results at 100 V/480 Hz and 75 V/240 Hz with DO-160G for a load of $R_L = 20 \Omega$. All the current harmonics at both frequencies are lower than the specified limits. The same observation is made when the load resistor value is halved (see Fig. 18).

B. Harmonic Spectrum (Experimental Results)

Similarly, Fig. 19 shows that none of the individual harmonics exceeds DO-160G limits while operating the test rig with a load resistance of $R_L = 20 \Omega$. Fig. 20 illustrates the effect of reducing the load resistor to 10Ω . Reassuringly, all current harmonics are below DO-160G specifications. The case of 480 Hz and $R_L = 10 \Omega$ represents maximum power delivered to the load. The IGBT stress at this condition is 16.5 A collector peak

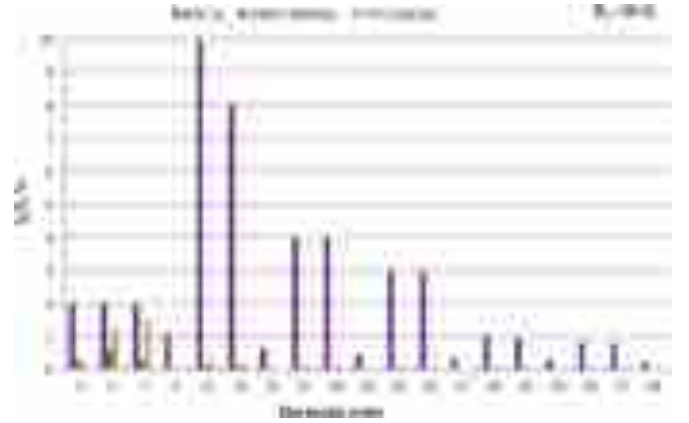


Fig. 18. Input current harmonic spectrum as a function of V_S/f_S ; simulated waveforms $R_L = 10 \Omega$.

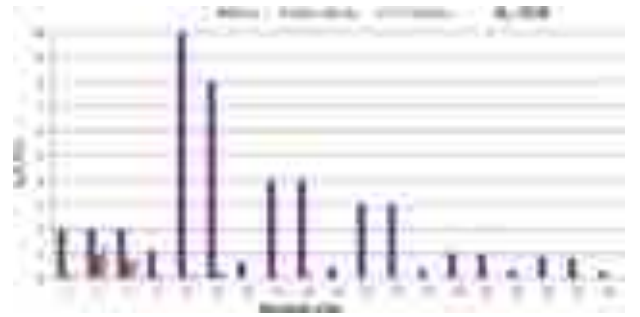


Fig. 19. Input current harmonic spectrum as a function of V_S/f_S ; experimental waveforms, $R_L = 20 \Omega$.

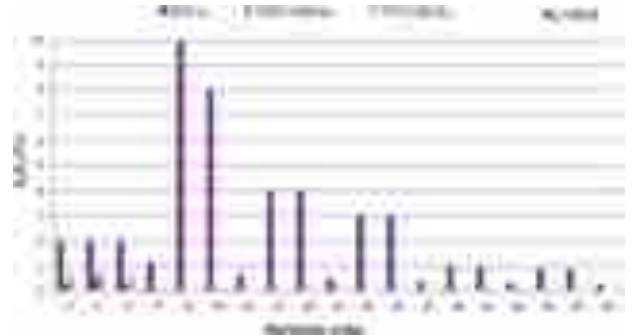


Fig. 20. Input current harmonic spectrum as a function of V_S/f_S ; experimental waveforms, $R_L = 10 \Omega$.

current and 687 V maximum collector-emitter voltage, which is equal to the capacitor voltage V_{cc} .

C. Efficiency Analysis

The FCSC-rectifier experiences on-state losses from the IGBTs (S_1 to S_6) and diodes (D_1 to D_6), and resistive losses caused by the internal parasitic resistors of the three capacitors (C_c). IGBT on-state losses occur only during the conduction period δ , thus the on-state losses for one IGBT can be expressed as

$$P_{\text{IGBT}} = \frac{\delta}{2\pi} * I_{\text{ph}} * V_{\text{CE on-state}} \quad (14)$$

where I_{ph} is the phase RMS current and $V_{\text{ce on-state}}$ is the on-state voltage of the IGBT. Switching losses can be ignored as the switching frequency for each IGBT is half the supply frequency

TABLE V
FCSC-RECTIFIER LOSSES AND EFFICIENCIES AT DIFFERENT
OPERATING CONDITIONS

Load	Supply voltage/frequency	δ	P_{total}	η_{cal}	η_m
$R_L = 10 \Omega$	100 V/480 Hz	0.00°	54.27 W	97.87%	94.16%
	75 V/240 Hz	86.41°	67.91 W	95.09%	92.60%
$R_L = 20 \Omega$	100 V/480 Hz	0.00°	25.17 W	98.55%	95.31%
	75 V/240 Hz	86.41°	35.57 W	96.23%	93.40%

f_s . Each of the diodes conducts for a period of π , thus the on-state losses for one diode is

$$P_{\text{diode}} = \frac{\pi}{2\pi} * I_{\text{ph}} * V_{\text{on-state}} = \frac{I_{\text{ph}} * V_{\text{on-state}}}{2} \quad (15)$$

with $V_{\text{on-state}}$ being the on-state voltage of the diode. The capacitor has a resistance of 66 m Ω , thus ohmic losses of the capacitor C_c can be estimated to

$$P_C = \frac{2\pi - \delta}{2\pi} * I_{\text{ph}}^2 * R_c. \quad (16)$$

Based on (14)–(16), total FCSC-rectifier losses were calculated (P_{total}) for four different scenarios as shown in Table V. Corresponding efficiency figures (η_{cal}) are also included in the table, calculated from the output powers for each scenario, showing efficiency values between 95% and 98.6%. The table also includes measured efficiency values (η_m); approximately 2% lower than the calculated efficiencies.

VII. CONCLUSION

This paper proposes a three-phase, variable-frequency, variable-voltage FCSC-rectifier circuit for MEA applications that does not require any filters in order to comply with current harmonics regulations such as DO-160G. The proposed rectifier is ideal for stand-alone systems such as powering the FADEC onboard an aircraft. The rectifier incorporates an IGBT controlled, three-phase series compensation circuit connected between a PM synchronous generator and a diode bridge rectifier. The reactance of the capacitor is continually varied (in line with the varying supply frequency) to match the generator inductive reactance and to achieve a minimum impedance resonant condition. This results in a sinusoidal ac current waveform in phase with the generator induced voltage over a wide range of operational voltages and frequencies.

Simulation and experimental results clearly show that the FCSC-rectifier is able to maintain a high value of power factor over a wide range of voltage and frequency values at different load conditions. The power factor improves with increasing load and supply frequency. All individual harmonics fell within the allowable limits when tested over a range of frequencies from 480 to 240 Hz. This occurred at all load conditions without the need for any additional filtering. In principle, the FCSC-rectifier can also be employed for other stand-alone aircraft VFG systems whenever there is a requirement for powering aircraft systems independently from an auxiliary power unit, as well as other stand-alone systems in nonaircraft applications.

REFERENCES

- [1] B. Sarlioglu and C. T. Morris, "More electric aircraft: Review, challenges, and opportunities for commercial transport aircraft," *IEEE Trans. Transp. Electric.*, vol. 1, no. 1, pp. 54–64, Jun. 2015.
- [2] X. Roboam, B. Sareni, and A. D. Andrade, "More electricity in the air: Toward optimized electrical networks embedded in more-electrical aircraft," *IEEE Ind. Electron. Mag.*, vol. 6, no. 4, pp. 6–17, Dec. 2012.
- [3] J. Rosero, J. Ortega, E. Aldabas, and L. Romeral, "Moving towards a more electric aircraft," *IEEE Aerosp. Electron. Syst. Mag.*, vol. 22, no. 3, pp. 3–9, Mar. 2007.
- [4] K. Peng, D. Fan, F. Yang, M. He, Y. Wang, and F. She, "Development and test evaluation of full authority digital electronic control system for auxiliary power unit based on electronic pump," in *Proc. IEEE Int. Conf. Signal Process., Commun. Comput.*, Hong Kong, 2016, pp. 1–4.
- [5] K. Beneda, "Development of a modular FADEC for small scale turbojet engine," in *Proc. IEEE Int. Symp. Appl. Mach. Intell. Informat.*, Herlany, Slovakia, 2016, pp. 51–56.
- [6] C. Cao, J. Shen, M. Luo, B. Yu, J. Wang, and Z. Hu, "FWorks: An integrated digital simulation platform for FADEC systems," in *Proc. IEEE Chin. Control Conf.*, Dalian, China, 2017, pp. 10316–10321.
- [7] I. Moir and A. Seabridge, *Aircraft Systems: Mechanical, Electrical, and Avionics Subsystems Integration*, Hoboken, NJ, USA: Wiley, 2008.
- [8] B. Chen, C. Li, Y. Li, and A. Wang, "Reliability analysis method of an aircraft engine FADEC system," in *Proc. Int. Conf. Rel., Maintainability Safety*, Chengdu, China, 2009, pp. 289–292.
- [9] L. Stoica *et al.*, "Design of a high temperature signal conditioning ASIC for engine control systems - HIGHTECS," in *Proc. IEEE Int. Symp. Circuits Syst.*, Melbourne, VIC, Australia, 2014, pp. 2117–2120.
- [10] J. Lutambo, J. Wang, H. Yue, and G. Dimirovsky, "Aircraft turbine engine control systems development: Historical perspective," in *Proc. IEEE Chin. Control Conf.*, Hangzhou, China, 2015, pp. 5736–5741.
- [11] Sean Gallagher, 2015. [Online]. Available: <https://arstechnica.co.uk/information-technology/2015/06/report-airbus-transport-crash-caused-by-wipe-of-critical-engine-control-data>
- [12] J. P. Morris and F. R. Lysinger, "Power source for aircraft engine controller systems," U.S. Patent 11 899 053, Mar. 2009.
- [13] P. Wheeler and S. Bozhko, "The more electric aircraft: Technology and challenges," *IEEE Electric. Mag.*, vol. 2, no. 4, pp. 6–12, Dec. 2014.
- [14] H. Abu-Rub, M. Malinowski, and K. Al-Haddad, *Power Electronics for Renewable Energy Systems, Transportation and Industrial Applications*, West Sussex, U.K.: IEEE Press, 2014.
- [15] K. Emadi and M. Ehsani, "Aircraft power systems: Technology, state of the art, and future trends," *IEEE Aerosp. Electron. Syst. Mag.*, vol. 15, no. 1, pp. 28–32, Jan. 2000.
- [16] A. J. Mitcham and J. J. A. Cullen, "Permanent magnet generator options for the more electric aircraft," in *Proc. Int. Conf. Power Electron., Mach. Drives*, Sante Fe, NM, USA, 2002, pp. 241–245.
- [17] C. R. Avery, S. G. Burrow, and P. H. Mellor, "Electrical generation and distribution for the more electric aircraft," in *Proc. 42nd Int. Univ. Power Eng. Conf.*, Brighton, U.K., 2007, pp. 1007–1012.
- [18] D. M. Miao, Y. Mollet, J. Gyselinc, and J. X. Shen, "DC voltage control of a wide-speed-range permanent-magnet synchronous generator system for more electric aircraft applications," in *Proc. IEEE Veh. Power Propulsion Conf.*, Hangzhou, China, 2016, pp. 1–6.
- [19] J. Chen, X. Zhang, and C. Wen, "Harmonics attenuation and power factor correction of a more electric aircraft power grid using active power filter," *IEEE Trans. Ind. Electron.*, vol. 63, no. 12, pp. 7310–7319, Dec. 2016.
- [20] *Environmental Conditions and Test Procedures for Airborne Equipment*, Standard DO-160G, RTCA, Inc., Washington, DC, USA, 2004.
- [21] J. Sun, "Conducted EMI modeling and mitigation for power converters and motor drives," in *Proc. ESA Workshop Aerosp. EMC*, Venice, Italy, 2012, pp. 1–6.
- [22] J. Brombach, M. Jordan, F. Grumm, and D. Schulz, "Converter topology analysis for aircraft application," in *Proc. Int. Symp. Power Electron. Elect. Drives Autom. Motion*, Sorrento, Italy, 2012, pp. 446–451.
- [23] A. Mallik and A. Khaligh, "Comparative study of three-phase buck, boost and buck-boost rectifier topologies for regulated transformer rectifier units," in *Proc. IEEE Transp. Electric. Conf. Expo.*, Dearborn, MI, USA, 2015, pp. 1–7.
- [24] A. Mallik, B. Faulkner, and A. Khaligh, "Control of a single-stage three-phase boost power factor correction rectifier," in *Proc. IEEE Appl. Power Electron. Conf. Expo.*, Long Beach, CA, USA, 2016, pp. 54–59.

- [25] X. Zhao, J. M. Guerrero, and X. Wu, "Review of aircraft electric power systems and architectures," in *Proc. IEEE Int. Energy Conf.*, Cavtat, Croatia, 2014, pp. 949–953.
- [26] A. O. Monroy, L.-H. Hoang, and C. Lavoie, "Modelling and simulation of a 24-pulse Transformer Rectifier Unit for more electric aircraft power system," in *Proc. Elect. Syst. Aircr., Railway Ship Propulsion*, Bologna, Italy, 2012, pp. 1–5.
- [27] F. Meng, L. Gao, S. Yang, and W. Yang, "Effect of phase-shift angle on a delta-connected autotransformer applied to a 12-pulse rectifier," *IEEE Trans. Ind. Electron.*, vol. 62, no. 8, pp. 4678–4690, Jun. 2015.
- [28] B. Sarlioglu, "Advances in AC-DC power conversion topologies for more electric aircraft," in *Proc. IEEE Transp. Electrific. Conf. Expo.*, Dearborn, MI, USA, 2012, pp. 1–6.
- [29] T. Yang, S. Bozhko, and G. Asher, "Active front-end rectifier modelling using dynamic phasors for more-electric aircraft applications," *IET Elect. Syst. Transp.*, vol. 5, no. 2, pp. 77–87, Jun. 2015.
- [30] G. Gong, M. L. Heldwein, U. Drogenik, J. Minibock, K. Mino, and J. W. Kolar, "Comparative evaluation of three-phase high-power-factor AC-DC converter concepts for application in future more electric aircraft," *IEEE Trans. Ind. Electron.*, vol. 52, no. 3, pp. 727–737, Jun. 2005.
- [31] D. Y. Komovskiy, "Comparative analysis of three-level PWM inverters for aircraft AC power systems," in *Proc. 17th Int. Conf. Young Spec. Micro/Nanotechnol. Electron Devices*, Erlagol, Russia, 2016, pp. 476–480.
- [32] M. Liserre, F. Blaabjerg, and S. Hansen, "Design and control of an LCL filter-based three-phase active rectifier," *IEEE Trans. Ind. Appl.*, vol. 41, no. 5, pp. 1281–1291, Sep/Oct. 2005.
- [33] K. Jalili and S. Bernet, "Design of LCL filters of active-front-end two-level voltage-source converters," *IEEE Trans. Ind. Appl.*, vol. 56, no. 5, pp. 1674–1689, May 2005.
- [34] L. F. W. de Souza, E. H. Watanabe, and J. E. da Rocha Alves, "Thyristor and gate-controlled series capacitors: A comparison of components rating," *IEEE Trans. Power Del.*, vol. 23, no. 2, pp. 899–906, Apr. 2008.
- [35] F. D. de Jesus, E. H. Watanabe, L. F. W. de Souza, and J. E. R. Alves, "SSR and power oscillation damping using gate-controlled series capacitors (GCSC)," *IEEE Trans. Power Del.*, vol. 22, no. 3, pp. 1806–1812, Jul. 2007.
- [36] H. A. Mohammadpour, M. M. Islam, E. Santi, and Y. J. Shin, "SSR damping in fixed-speed wind farms using series FACTS controllers," *IEEE Trans. Power Del.*, vol. 31, no. 1, pp. 76–86, Feb. 2016.
- [37] I. Matsumoto and S. Nomura, "Power factor correction of large current line commutated converters using variable series capacitors," in *Proc. 15th Eur. Conf. Power Electron. Appl.*, Lille, France, 2013, pp. 1–9.
- [38] N. G. Hingorani and L. Gyugyi, *Understanding FACTS: Concepts and Technology of Flexible AC Transmission System*. New York, NY, USA: IEEE Press, 2000.
- [39] R. Hunter and G. Elliot, *Wind-Diesel Systems: A Guide to the Technology and Its Implementation*. Cambridge, U.K.: Cambridge Univ. Press, 1994.
- [40] T. Al-Mhana, V. Pickert, and B. Zahawi, "FCSC converter with symmetrical short duty cycle for variable frequency applications," in *Proc. 7th IET Int. Conf. Power Electron., Mach. Drives*, Manchester, U.K., 2014, pp. 1–5.
- [41] T. Al-Mhana, B. Zahawi, and V. Pickert, "Symmetrical duty cycle control for FCSC converter for wave energy applications," in *Proc. 9th Int. Symp. Commun. Syst., Netw. Digit. Sign.*, Manchester, U.K., 2014, pp. 56–60.
- [42] N. J. Baker, D. J. Smith, M. C. Kulan, and S. Turvey, "Design and performance of a segmented stator permanent magnet alternator for aerospace," *IEEE Trans. Energy Convers.*, vol. 33, no. 1, pp. 40–48, Mar. 2018.
- [43] N. J. Baker, D. J. Smith, M. C. Kulan, and S. Turvey, "Design and performance of a segmented stator permanent magnet alternator for aerospace," in *Proc. IET Int. Conf. Power Electron., Mach. Drives*, Manchester, U.K., 2014, pp. 1–5.
- [44] L. Jinjun, T. G. Wilson, R. C. Wong, R. Wunderlich, and F. C. Lee, "A method for inductor core loss estimation in power factor correction applications," in *Proc. 17th IEEE Appl. Power Electron. Conf. Expo.*, Dallas, TX, USA, 2002, pp. 439–445.
- [45] W. U. N. Fernando, M. Barnes, and O. Marjanovic, "Direct drive permanent magnet generator fed AC-DC active rectification and control for more-electric aircraft engines," *IET Elect. Power Appl.*, vol. 5, pp. 14–27, 2011.



Tahani Al-Mhana (S'11–M'18) received the B.Sc. degree from Mosul University, Mosul, Iraq, in 1992, and the M.Sc. degree from the University of Technology, Baghdad, Iraq, in 2000, both in electrical engineering, and the Ph.D. degree in electrical and electronic engineering from Newcastle University, Newcastle upon Tyne, U.K., in 2016.

Since 1992, she has been with the Department of Electrical Engineering, University of Babylon, Hilla, Iraq, where she is currently a Lecturer in electrical machines and power electronics. Her research interests include power electronics and its applications such as in more-electric aircraft, renewable energy, electrical machines control, power factor correction, series compensations, and harmonics.



Volker Pickert (M'04) received the Dipl.Ing. degree in electrical and electronic engineering from Rheinisch-Westfaelische Technische Hochschule, Aachen, Germany, in 1994, and the Ph.D. degree in power electronics from Newcastle University, Newcastle upon Tyne, U.K., in 1997.

From 1998 to 1999, he was an Application Engineer with Semikron GmbH, Nuremberg, Germany, and from 1999 to 2003, he was a Group Leader with Volkswagen AG, Wolfsburg, Germany, responsible for the development of electric drives for electric vehicles. In 2003, he was a Senior Lecturer with the Electrical Power Research Group, Newcastle University, and in 2011, he became a Full Professor of power electronics. In 2012, he became the Head of the Electrical Power Research Group. He has authored or coauthored more than 130 book chapters, journal, and conference papers in the area of power electronics and electric drives. His current research interests include power electronics for automotive applications, thermal management, health monitoring techniques, and advanced nonlinear control.

Dr. Pickert was the recipient of the IMarEST Denny Medal for the best article in the *Journal of Marine Engineering* in 2011. He was the Chairman of the biannual international IET conference on Power Electronics, Machines and Drives in 2010 in Brighton and he is the active Editor-in-Chief of the *IET Power Electronics* journal.



David J. Atkinson received the B.Sc. degree in electrical and electronic engineering from Sunderland Polytechnic, Sunderland, U.K., in 1978, and the Ph.D. degree in electrical and electronic engineering from Newcastle University, Newcastle upon Tyne, U.K., in 1991.

He is a Senior Lecturer with the Drives, Electrical Power Group, School of Engineering, Newcastle University. Prior to his university appointment in 1987, he spent 17 years in the electronics industry including periods with NEI Electronics and British Gas Corporation. His research interests include electrical drive systems and power electronics control for new and renewable energy systems.

Dr. Atkinson was the recipient of the IEE Power Premium Prize.



Bashar Zahawi (M'96–SM'04) received the B.Sc. and Ph.D. degrees in electrical and electronic engineering from Newcastle University, Newcastle upon Tyne, U.K., in 1983 and 1988, respectively.

From 1988 to 1993, he was a Design Engineer with a U.K., manufacturer of large variable speed drives and other power conversion equipment. He was appointed as a Lecturer in electrical engineering at the University of Manchester, Manchester, U.K., in 1994, and was a Senior Lecturer with the School of Electrical and Electronic Engineering, Newcastle University, from 2003 to 2014. Since 2014, he has been with the Department of Electrical and Computer Engineering, Khalifa University, Abu Dhabi, United Arab Emirates, where he is currently a Professor in electrical power engineering. His research interests include, power conversion, renewable energy, optimization methods, and the application of nonlinear dynamical methods to electrical circuits and systems.

Dr. Zahawi was a recipient of the Crompton Premium awarded by the Institution of Electrical Engineers, U.K., and the Denny Medal awarded by the Institute of Marine Engineering, Science and Technology. He is currently the Chairman of the IEEE Power and Energy Society United Arab Emirates Chapter.